

## Original Article

# Synthesis, chromism, antimicrobial activity, molecular docking, and pharmacokinetics of novel molecular switchable hydrazones

Salhah D. Al-Qahtani<sup>a</sup>, Ghadah M. Al-Senani<sup>a</sup>, Maryam Aldoghaim<sup>b,\*</sup>

<sup>a</sup>Department of Chemistry, College of Science, Princess Nourah bint Abdulrahman University, P.O. Box 84428, Riyadh 11671, Saudi Arabia

<sup>b</sup>Department of Chemistry, College of science, King Faisal University, Al-ahsa 31982, Saudi Arabia

## ARTICLE INFO

**Keywords:**  
Antimicrobial  
Molecular docking  
Solvatochromism  
Swiss ADME  
Tricyanofuran-based hydrazone

## ABSTRACT

A series of novel tricyanofuran-hydrazone chromophores were synthesized and characterized by different spectroscopic techniques. The prepared hydrazones displayed solvatochromic activity in different organic solvents. The tricyanofuran-hydrazone was imprinted onto a paper strip as an optical solid-state sensor for aqueous and gaseous ammonia. Due to their reversible halochromism-driven molecular switching, the hydrazone dyes showed variable sensitivity towards different concentrations of aqueous ammonia. The strong electron-withdrawing tricyanofuran fragment promotes a proton transfer from the hydrazone moiety to ammonia, which allows for the recognition of ammonia vapor. The resulting paper sensor demonstrated a reversible sensitivity to ammonia vapor. Using the minimum inhibitory concentration (MIC) method, the dinitro-substituted chromophore showed the strongest antibacterial activity. It was effective against *A. fumigatus*, *C. albicans*, *E. coli*, *S. pneumoniae*, and *S. aureus*, with MIC values of <226, <198, <122, <71, and <38, respectively. Thus, the dinitro-substituted chromophore appears to be a promising antibacterial agent. The theoretical molecular docking study of the produced series against a protein of interest (PDB: 1lnz) was performed to assign the binding and type of interaction between ligand and protein amino acids. The pharmacokinetic properties of potential drug candidates for the synthesized chromophores were simulated to determine their efficacy and safety profiles.

## 1. Introduction

Hydrazones have been significant agents in medicinal chemistry owing to their efficient biological action against various diseases, such as inflammation, cancer, leishmaniasis, and Alzheimer's [1-3]. Hydrazones have been utilized in biotechnology to couple drugs for the treatment of cancer cells [4]. They have been used as anti-tuberculosis, analgesic, anti-inflammatory, anti-HIV, anti-tumor, anticonvulsant, and antimicrobial agents [5-7]. They have been applied as crucial agents in drug delivery systems, dynamic combinatorial chemistry, hole-transporting materials, metal and covalent organic frameworks, and coordination ligands for organocatalysis [8-10]. Khat tab *et al.* [11] recently reported the development of switchable hydrazones with thermo chromic and halochromic properties. Ammonia is the most prominent alkaline gas in the context of industrial technology [12,13]. Ammonia is extremely toxic and has a significant technological turnover as an intermediary in the formation of synthetic polymers, explosives, fertilizers, and textiles, making its detection particularly interesting. Pure ammonia is used as an industrial refrigerant [14]. Detection of ammonia has been significant in numerous fields, such as foodstuffs, healthcare, electronics, environment, and quality control [15-17]. Ammonia has shown harmful effects on human health, even at low concentrations. Thus, the development of a sensitive and quick method for determining ammonia concentration is highly in demand. When the

concentration of ammonia gas exceeds 1 ppm, it can cause irritation to the throat, eyes, and nose. Exposure to ammonia concentration of <300 ppm is highly dangerous and can cause irreversible lung damage, serious burning of skin, and eye irritation, whereas exposure to ammonia gas of >300 ppm causes death. Furthermore, the highest authorized amount in a workplace for an overall 8-hr exposure is just 25 ppm. At aerial quantities of roughly 15-28% by volume, ammonia is also combustible [18-20]. Thus, numerous sensors were reported for the determination of ammonia, such as solid-state copper sulfide films, tellurium thin films, thin films of copper bromide, acrylic acid doped polyaniline, and nanoporous anodized alumina [21-24]. However, these sensory materials show a detection limit below the ppm level. Additionally, they frequently require complicated procedures, including high working temperatures, trained personnel, and/or complicated operations [25]. Thus, it has been significant to develop a simple and reversible ammonia sensor with high sensitivity at the ppb level. Consequently, an increase in the surface area of a sensor will boost its sensitivity. High adsorption and rapid diffusion throughout the mesh are triggered by the high surface area of a sensor [26].

Herein, we describe a straightforward procedure for creating a reversible optical molecular switching probe consisting of a donor hydrazone moiety in conjugation with an acceptor tricyanofuran (TCF) moiety. The deprotonated hydrazone group functions as a  $\pi$ -bridge in a

### \*Corresponding author:

E-mail address: [maldoghaim@kfu.edu.sa](mailto:maldoghaim@kfu.edu.sa) (M. Aldoghaim)

Received: 25 January, 2025 Accepted: 11 February, 2025 Epub Ahead of Print: 07 April 2025 Published: 17 April 2025

DOI: 10.25259/AJC.72\_2025

push-pull system. Additionally, it can act as a donor group itself when bonded with a strong electron-withdrawing group [27].

## 2. Materials and Methods

### 2.1. Materials and methods

All chemical agents and organic solvents (analytical grade) were obtained from Merck (Germany). Melting points were measured in °C without correction using an electrothermal tool. Infrared spectra were reported by a Bruker Vectra 33 (United States). A Perkin-Elmer 2400 (Norwalk, United States) was used to conduct the elemental analysis (C, H, N). A HP-8453 spectrophotometer (Hewlett-Packard, United States) was used to measure the UV-visible absorption spectra. NMR spectra were determined by a BRUKER AVANCE 400 MHz (Karlsruhe, Germany). A Quanta 250 FEG scanning electron microscope (Czech Republic) was employed to explore the morphology of the hydrazone-imprinted paper strips.

### 2.2. Sensor testing and reversibility

A glass vial (10 mL) was filled with approximately 5 mL of aqueous ammonia. When the sensory paper was placed close to the nozzle of the glass vial, a rapid color change occurred from yellow to purple. Then, the purple paper strip was found to revert to its yellow color after a few seconds in the air. The abovementioned procedure was performed for numerous cycles, and the absorption spectra were collected after each cycle using an UltraScanPro spectrophotometer (HunterLab, United States).

### 2.3. Synthesis and characterization

#### 2.3.1. Synthesis of tricyanofuran (TCF)

In a round bottom flask set in a water-bath at 25°C, a piece of metallic sodium (75 mg, 3.25 mmol) was dissolved in absolute ethanol (2.5 mL). Then, malononitrile (3 g, 45 mmol) and 3-hydroxy-3-methylbutanone (2.25 g, 22 mmol) were added to the produced solution of sodium ethoxide. The solution was stirred for 1 hr, and then absolute ethanol (10 mL) was poured into the reaction system. The resultant combination was subjected to reflux for 1 hr, cooled in a fridge at 4°C, filtered under vacuum, rinsed with cold ethanol, and then air dried to produce off-white crystals (2.57 g; 58%). mp 202-203°C. <sup>1</sup>H NMR (400 MHz, CDCl<sub>3</sub>): 1.65 (s, 6H), 2.37 (s, 3H).

#### 2.3.2. General synthesis of hydrazone (1-5)

In a round bottom flask set in an ice bath at 0-5°C, a combination of arylamine (2.5 mmol), water (1.5 mL), and HCl (1.5 mL) was stirred. An aqueous solution of sodium nitrite (2.5 mmol) in distilled water (1 mL) was slowly dropped into the solution at 0-5°C, and then the resultant combination was stirred for 20 mins at 0-5°C to produce the corresponding diazonium salt. A solution of tricyanofuran (2.5 mmol) in acetonitrile (2.5 mL), sodium acetate (0.75 g), and acetic acid (1 mL) was cooled to 0-5°C and then slowly poured into the aforementioned diazonium solution. The resulting solution was stirred for 30 mins in an ice-bath at 0-5°C. The product was filtered under vacuum, washed with distilled water, and air-dried to generate solid powder.

#### Preparation of tricyanofuran hydrazone (1)

Hydrazone (1) was synthesized from tricyanofuran (500 mg, 2.5 mmol) and aniline (250 mg, 2.5 mmol) and recrystallized from CHCl<sub>3</sub> to generate orange powder (0.65 g; 74%). mp 218°C; <sup>1</sup>H NMR (400 MHz, DMSO-d<sub>6</sub>): 1.78 (s, 6H), 7.14 (t, 1H), 7.28 (d, 2H), 7.43 (t, 2H), 7.82 (s, 1H), 12.65 (s, 1H); <sup>13</sup>C NMR (400 MHz, DMSO-d<sub>6</sub>): 26.62, 98.83, 111.38, 112.81, 113.57, 114.87, 115.62, 125.08, 126.67, 128.77, 130.35, 137.68, 142.44, 172.62, 177.68; IR (ν/cm<sup>-1</sup>): 1627 (C=N), 2227 (CN), 3304 (NH); Elemental contents: Calculated: C 67.32; H 4.32; N 23.09, Found C 67.56; H 4.52; N 23.02.

#### Preparation of tricyanofuran hydrazone (2)

Hydrazone (2) was synthesized from tricyanofuran (500 mg, 2.5 mmol) and 4-methylaniline (440 mg, 2.5 mmol) and recrystallized from chloroform/methanol to generate an orange solid (880 mg; 61%). mp 218°C; <sup>1</sup>H NMR (400 MHz, DMSO-d<sub>6</sub>): 1.81 (s, 6H), 2.32 (s, 3H), 7.21 (d, 2H), 7.24 (d, 2H), 7.79 (s, 1H), 12.67 (s, 1H); <sup>13</sup>C NMR (400 MHz, DMSO-d<sub>6</sub>): 21.04, 26.73, 98.57, 111.60, 113.02, 113.78, 115.86, 124.45, 130.80, 134.85, 140.21, 172.29, 177.70; IR (ν/cm<sup>-1</sup>): 1581 (C=N), 2208 (CN), 2854 (CH aromatic), 2905 (CH aliphatic), 3393 (NH); Elemental contents: Calculated: C 68.13; H 4.76; N 22.07, Found C 68.19; H 4.90; N 22.14.

#### Preparation of tricyanofuran hydrazone (3)

Hydrazone (3) was synthesized from tricyanofuran (500 mg, 2.5 mmol) and 4-octylaniline (510 mg, 2.5 mmol) and recrystallized from chloroform/methanol to generate an orange solid (955 mg; 86%). mp 211°C; <sup>1</sup>H NMR (400 MHz, DMSO-d<sub>6</sub>): 0.91 (s, 3H), 1.63 (s, 12H), 1.82 (s, 6H), 2.01 (m, 2H), 7.25 (d, 2H), 7.26 (d, 2H), 7.84 (s, 1H), 12.65 (s, 1H); <sup>13</sup>C NMR (400 MHz, DMSO-d<sub>6</sub>): 21.37, 24.08, 25.02, 25.97, 26.27, 27.98, 97.97, 110.42, 112.65, 113.92, 115.41, 124.86, 130.24, 134.95, 140.04, 172.55, 177.62; IR (ν/cm<sup>-1</sup>): 1573 (C=N), 2218 (CN), 2895 (CH aromatic), 2922 (CH aliphatic), 3393 (NH); Elemental contents for (C<sub>25</sub>H<sub>29</sub>N<sub>5</sub>O; 415.31): Calculated: C 75.18; H 7.23; N 18.37, Found C 75.09; H 7.28; N 18.19.

#### Preparation of tricyanofuran hydrazone (4)

Hydrazone (2) was synthesized from tricyanofuran (500 mg, 2.5 mmol) and 4-trifluoromethyl aniline (400 mg, 2.5 mmol) and recrystallized from ethanol/CHCl<sub>3</sub> to generate a red solid (605 mg; 80%). mp 227°C; <sup>1</sup>H NMR (400 MHz, DMSO-d<sub>6</sub>): 1.81 (s, 6H), 7.38 (d, 2H), 7.99 (s, 1H), 8.26 (d, 2H), 12.79 (s, 1H); <sup>13</sup>C NMR (400 MHz, DMSO-d<sub>6</sub>): 26.33, 99.27, 99.41, 110.84, 112.35, 113.11, 115.16, 126.50, 129.16, 142.83, 147.79, 171.88, 177.35; IR (ν/cm<sup>-1</sup>): 1579 (C=N), 2228 (CN), 3277 (NH); Elemental contents: Calculated: C 58.62; H 3.47; N 24.13, Found C 58.81; H 3.51; N 24.27.

#### Preparation of tricyanofuran hydrazone (5)

Hydrazone (3) was synthesized from tricyanofuran (500 mg, 2.5 mmol) and 3,5-dinitroaniline (460 mg, 2.5 mmol) and crystallized from *n*-propanol/CHCl<sub>3</sub> to generate a reddish powder (585 mg; 68%). mp 238°C; <sup>1</sup>H NMR (400 MHz, DMSO-d<sub>6</sub>): 1.81 (s, 6H), 7.65 (d, 1H), 8.23 (dd, 1H), 8.37 (d, 1H), 8.58 (s, 1H), 12.10 (s, 1H); <sup>13</sup>C NMR (400 MHz, DMSO-d<sub>6</sub>): 25.82, 110.71, 111.83, 112.59, 115.47, 124.55, 125.97, 132.27, 142.05, 171.15, 176.83; IR (ν/cm<sup>-1</sup>): 1521 and 1332 (NO<sub>2</sub>), 1579 (C=N), 2235 (CN), 3259 (NH); Elemental contents: Calculated: C 51.91; H 2.82; N 24.93, Found C 51.90; H 2.69; N 24.75.

### 2.4. Antimicrobial assessment

Using the inhibition zone method [28,29], the antimicrobial evaluation for tricyanofuran-hydrazone chromophores was studied against different bacterial panels, including *B. subtilis* (ATCC 6633) and *S. aureus* (ATCC 29213) as Gram positive bacteria, and *E. coli* (ATCC 25922) and *S. typhimurium* (ATCC 14028) as Gram negative bacteria. Amoxicillin was applied as a reference drug; the antimicrobial properties were determined via the minimum Inhibitory concentration (MIC) procedure. The inhibition zone diameter (IZD) was determined over three trials, using dimethylsulfoxide (DMSO) as a solvent with no inhibitory effects.

### 2.5. Molecular docking

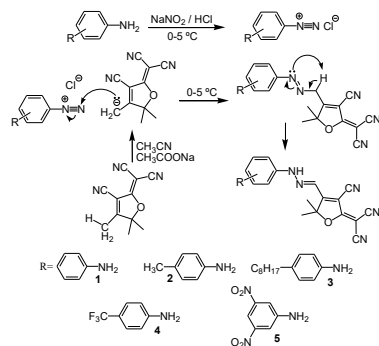
The X-ray crystal structure elucidation of protein data bank (PDB) entry for this complex (PDB ID: 1LNZ) finished the molecular structure and function of the GTP binding protein complexation a lot improved [30]. Because they are so imperative for signaling, protein movement, processing, and governing the cell cycle, guanosine triphosphate (GTP)-binding proteins have grown to be found in all known forms of life.

The docking calculations were achieved using computational study by M.O.E. program to further examine the molecular interactions. Hydrogen bonds are particularly important in biology because they regulate the structural integrity and functional dynamics of macromolecules. Identifying hydrogen bond interactions has been the main goal of ligand-receptor binding studies to learn more about complex molecular signaling and recognition pathways.

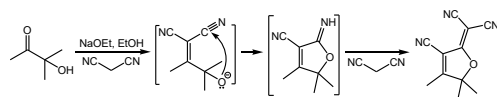
### 3. Results and Discussion

#### 3.1. Synthesis and chemistry

**Scheme 1** illustrates a simple method used to synthesize TCF-hydrazone sensor chromophores. Preparation of the tricyanofuran intermediate gave a 58% yield according to an early procedure [26]. In comparison to a hydrogen atom on a carbon next to electron-donating units, hydrogen on a carbon next to a strongly electron-withdrawing substituent(s) in a particular molecule are significantly highly acidic [31]. Herein, a carbanion is formed by the abstraction of a proton from the active methyl on the TCF heterocycle. This carbanion is stabilized by the highly electron-withdrawing cyano substituents on TCF, as shown in **Scheme 2**. **Table 1** displays the optical properties of the TCF-hydrazone chromophores in nonpolar and polar organic solvents. When exposed to different solvents, the colors of these TCF-H chromophores ranged between yellow, orange, red, and purple, demonstrating high solvatochromism. These results pointed to a charge delocalization in a strongly allowed  $\pi$ - $\pi^*$  transition [32]. When the hydrogen of N-H is eliminated, a hydrazone anion that exhibits prolonged conjugation is generated. The hydrazone anion acts as an electron donor, whilst TCF



**Scheme 1.** Synthesis of hydrazones.



**Scheme 2.** Synthesis of TCF heterocycle via Knoevenagel condensation.

**Table 1.** Spectroscopic data of TCFH in various solvents.

Solvent	$E_t$ (30 kcal mol <sup>-1</sup> ) [33]	$\lambda_{max}$ (nm)				
		R=H	R=4-CH <sub>3</sub>	R=4-(CH <sub>2</sub> ) <sub>7</sub> CH <sub>3</sub>	R=4-CF <sub>3</sub>	R=3,5-(NO <sub>2</sub> ) <sub>2</sub>
Methanol	55.4	475	485	471	464	473
<i>n</i> -Propanol	50.7	478	499	467	467	465
Ethanol	51.9	472	487	456	470	478
Acetone	42.2	468	480	455	482	493
DMSO	45.1	486	491	453	539	502
DMF	43.2	477	476	464	525	565
Dioxane	36.0	464	473	462	477	457
THF	37.4	471	481	460	483	453
Toluene	33.9	464	477	455	469	460

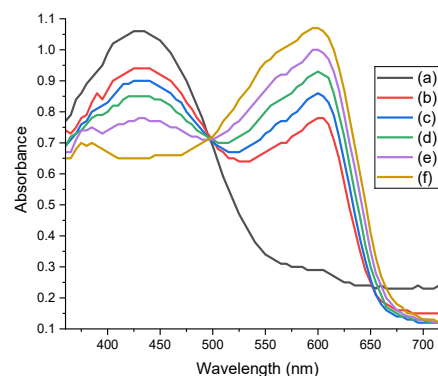


**Figure 1.** Absorption spectra of hydrazone-imprinted paper strip for detection of ammonia at different concentrations; (a) 50 parts per billion (ppb), (b) 100 ppb, (c) 150 ppb, (d) 200 ppb, (e) 250 ppb, and (f) 300 ppb.

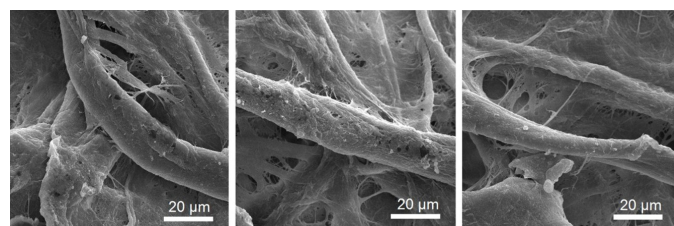


**Figure 2.** SEM images of hydrazone-imprinted paper strip at different positions. SEM: Scanning electron microscopy.

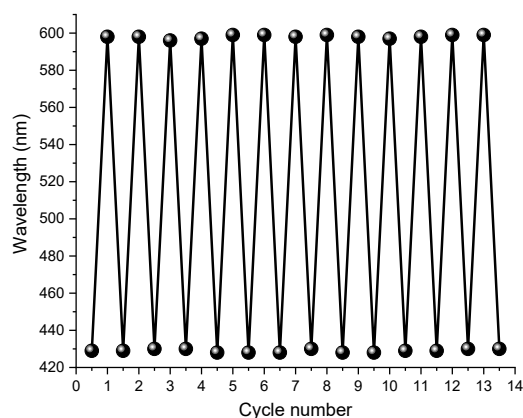


**Figure 3.** Reversibility of hydrazone-imprinted paper strip for detection of ammonia.

moiety serves as an electron acceptor. A straightforward azo-coupling synthesis pathway was performed between an active methyl-containing tricyanofuran and a diazonium chloride.

The tricyanofuran-hydrazone probe [4] was imprinted onto a paper strip and exposed to ammonia gas. **Figure 1** shows the absorption spectra of the hydrazone-imprinted paper at different concentrations of ammonia to indicate a gradual colorimetric shift from yellow to purple upon increasing the ammonia concentrations from 50 ppb to 300 ppb, respectively. **Figure 2** displays scanning electron microscope (SEM) images of a hydrazone-imprinted paper strip. The current sensor paper displayed high reversibility, as illustrated in **Figure 3**. This result was associated with a bathochromic shift from 429 nm (yellow) to 598 nm (purple). These results pointed to a charge delocalization due to a hydrogen abstraction of N-H, generating a hydrazone anion with extended conjugation, as shown in **Figure 4**.

#### 3.2. Antimicrobial properties

Insight the antibacterial behavior of the tricyanofuran-hydrazone chromophores (**Table 2**). Because it had MIC values of < 56 µg/mL for

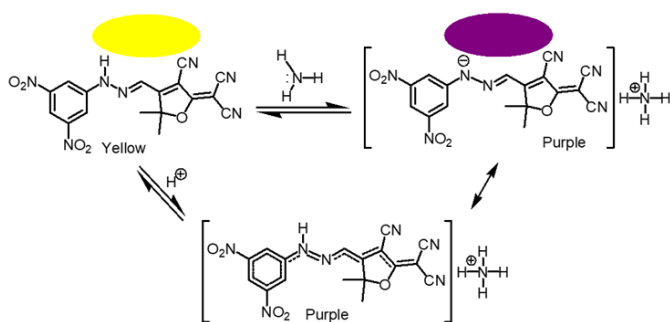


**Figure 4.** Solid-state reversible sensor displaying a change in color from yellow to purple when exposed to ammonia vapor.

**Table 2.** Minimum inhibition concentration (MIC) screening for tricyanofuran-hydrazone chromophores.

Compound	MIC ( $\mu\text{g/mL}$ )					
	<i>S. aureus</i>	<i>S. pneumoniae</i>	<i>E. coli</i>	<i>S. typhimurium</i>	<i>C. albicans</i>	<i>A. fumigatus</i>
(1) R= H	< 56	< 66	< 152	< 47	< 244	< 239
(2) R= 4- $\text{CH}_3$	< 47	< 59	< 134	< 38	< 238	< 213
(3) R= 4-( $\text{CH}_2$ ) <sub>7</sub> $\text{CH}_3$	< 44	< 78	< 129	< 43	< 249	< 261
(4) R= 4- $\text{CF}_3$	< 51	< 61	< 143	< 59	< 203	< 243
(5) R= 3,5-( $\text{NO}_2$ ) <sub>2</sub>	< 38	< 71	< 122	-	< 198	< 226
Penicillin	< 40	< 63	< 124	< 30	-	-
Fluconazole	-	-	-	-	< 212	< 221

Fluconazole and Ampicillin are standard drugs.

*S. aureus*, < 66  $\mu\text{g/mL}$  for *S. pneumoniae*, < 152  $\mu\text{g/mL}$  for *E. coli*, < 47  $\mu\text{g/mL}$  for *S. typhimurium*, < 244  $\mu\text{g/mL}$  against *C. albicans*, and < 239  $\mu\text{g/mL}$  for *A. fumigatus*, chromophore 1 was classified as having strong antibacterial performance. Meanwhile, chromophore 2 exhibited more antimicrobial effectiveness compared to chromophore 1. It displayed MIC values of < 47  $\mu\text{g/mL}$  for *S. aureus*, < 59  $\mu\text{g/mL}$  for *S. pneumoniae*, < 134  $\mu\text{g/mL}$  for *E. coli*, < 38  $\mu\text{g/mL}$  for *S. typhimurium*, < 238  $\mu\text{g/mL}$  for *C. albicans*, and < 213  $\mu\text{g/mL}$  for *A. fumigatus*. Provisionally, it had a stronger inhibitory influence on gram-positive bacteria. Low MIC values (< 44  $\mu\text{g/mL}$ ) for chromophore 3 showed respectable results. These values were < 43  $\mu\text{g/mL}$  for *S. typhimurium*, < 129  $\mu\text{g/mL}$  for *E. coli*, < 249  $\mu\text{g/mL}$  for *C. albicans*, < 78  $\mu\text{g/mL}$  for *S. pneumoniae*, and < 261  $\mu\text{g/mL}$  for *A. fumigatus*. In addition, its effectiveness against Gram-negative bacteria was remarkable but rather less influential than chromophore 2. Furthermore, chromophore 4 demonstrated striking antimicrobial effectiveness, although slightly less potent than chromophores 2 and 3. It exhibited MIC value of < 61  $\mu\text{g/mL}$  for *S. pneumoniae*, < 203  $\mu\text{g/mL}$  for *C. albicans*, < 51  $\mu\text{g/mL}$  for *S. aureus*, < 59  $\mu\text{g/mL}$  for *S. typhimurium*, < 143  $\mu\text{g/mL}$  for *E. coli*, and < 243  $\mu\text{g/mL}$  against *A. fumigatus*. While it demonstrated effectiveness against a wide variety of bacteria, its strength was not as prominent as that of other chromophores. Moreover, chromophore 5 had the highest antibacterial activity compared to all other chromophores. It displayed MIC values of < 38  $\mu\text{g/mL}$  for *S. aureus*, < 122  $\mu\text{g/mL}$  for *E. coli*, < 71  $\mu\text{g/mL}$  for *S. pneumoniae*, < 198  $\mu\text{g/mL}$  for *C. albicans*, and < 226  $\mu\text{g/mL}$  for *A. fumigatus*. Furthermore, it displayed extraordinary inhibitory properties against Gram-negative and Gram-positive bacteria, emphasizing its wide-ranging antimicrobial effectiveness.

### 3.3. Structural-activity relationship

The structural-activity relationship (SAR) of the synthesized tricyanofuran-hydrazone chromophores may be understood by examining the changes in their chemical structures and how these relate to their antibacterial activities. Chromophore 1, which contains

a phenyl-hydrazone moiety, showed modest antimicrobial performance against Gram-negative and Gram-positive bacteria. The existence of a phenyl group may enhance the interaction with bacterial cell components, resulting in increased effectiveness towards *S. aureus* and *S. pneumoniae*. Additionally, the substitution of the phenyl ring by a *p*-tolyl group in chromophore 2 may result in advantageous interactions with bacterial pathogens, hence enhancing its effectiveness towards *E. coli* and *S. typhimurium*. Chromophore 3, distinguished by the presence of a 4-octylphenyl group, exhibited a persistent ability to struggle Gram-positive bacteria. The inclusion of a lengthier alkyl chain might potentially increase its ability to penetrate cell membranes and bind more strongly, hence enhancing its effectiveness toward *S. pneumoniae*. Furthermore, chromophore 4, which contains a 4-(trifluoromethyl) phenyl group, exhibited strong antimicrobial activity for Gram-negative and Gram-positive bacteria. The inclusion of a trifluoromethyl group can increase the chromophore ability (4) to dissolve in fats and its electron density, thereby enhancing its effectiveness toward *E. coli* and *S. typhimurium*. In addition, the fifth chromophore, which had a modified hydrazinylidene moiety with a 3,5-dinitrophenyl group, exhibited remarkable antimicrobial efficiency against Gram-positive bacteria. The existence of two nitro groups causes an electron-withdrawing effect, enhancing molecular interactions and cellular uptake, leading to this activity. As a result, this chromophore shows potent activity towards both *S. pneumoniae* and *S. aureus*. It can be concluded that the SAR analysis shows how certain structural features, like aromatic substituents and electron-withdrawing groups, make the chromophores more effective against microbes. By making more changes to the structure based on SAR principles, it might be possible to create new antimicrobials that work better and are less harmful.

### 3.4. Molecular docking

The binding interactions of the examined chromophores toward the target PDB-1lnz protein were uncovered by the molecular docking reproductions. Simultaneously, the findings revealed unique trends across the tricyanofuran-hydrazone chromophores, providing insights into their unique binding affinities and critical intermolecular interactions. However, chromophore 3 revealed a high binding affinity ( $S = -7.2496$  kcal/mol) through hydrogen bonding between nitrile groups N28 and Asn282 over an intermolecular distance of 3.49 Å (Figure 5).

However, the binding affinity of chromophore 4, which was measured at  $S = -6.5070$  kcal/mol, suggested a modest but significant interaction with the target protein. The H-acceptor between the nitrile groups nitrogen 24 and Val169 was the main emphasis of the interaction. This interaction is crucial because it helps to preserve the ligand in place within the binding pocket. In addition, chromophore 4 has a moderate affinity for the target PDB-1lnz protein, as evidenced by its somewhat lower binding affinity when compared to chromophores 3 and 5. However, the interaction side view of chromophore 4 demonstrates its significance in ligand-protein bindings. Likewise, the H-acceptor may seem to be the main form of contact for chromophore 4, but other aspects, such as  $\pi$ -interactions and hydrogen bond forces (donor and acceptor), must also be considered. Although less so than hydrogen bonding, these other interactions may help keep the ligand-protein complex together (Figure 6).

Though, the high binding affinity (-7.0952 kcal/mol) of chromophore 5 further highlighted the importance of targeted ligand-protein bindings. The main binding interaction is the creation of hydrogen bonding between Lys283 and N22 in the nitrile group (Figure 7).

This proves that H-acceptor is critical for ligand stabilization in the binding pocket. In disparity, the binding affinities of chromophores 3, 5, and 1 were slightly lower than those of chromophores 2 and 4. Nevertheless, there were still significant interactions between the target protein and its variants. Chromophore 1 typifies an interaction that involves hydrogen bonds between the N11 of the hydrazone moiety and Asp245, as well as between the nitrogen 24 of the nitrile group and Val 169 (Figure 8).

The phenyl-ring and Gly251 interacted with each other like in Chromophore 2. Moreover, Asp 257 and N11 of the hydrazone moiety interacted with each other through an H-donor bond (Figure 9).

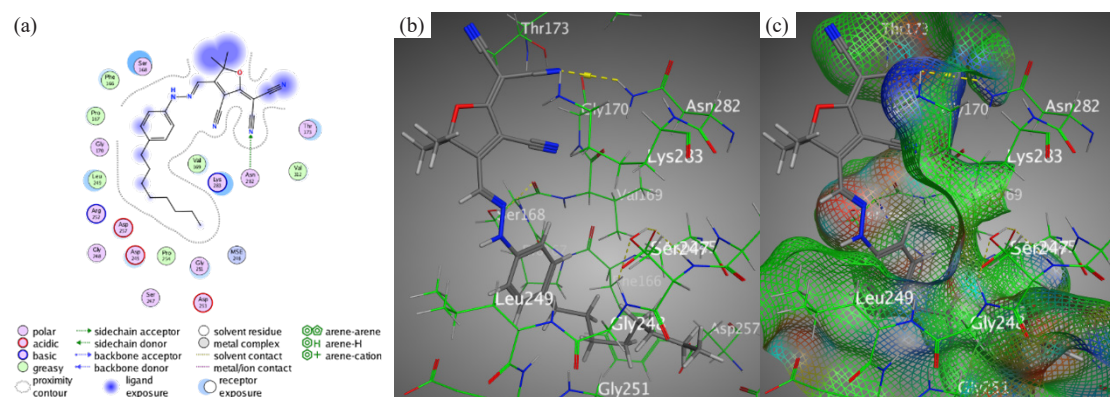


**Figure 5.** Docking interactions between chromophore 3 and PDB: 1lnz. (a) Two dimensions, (b) Three dimensions, (c) Surface Mapping. PDB: Protein data bank.

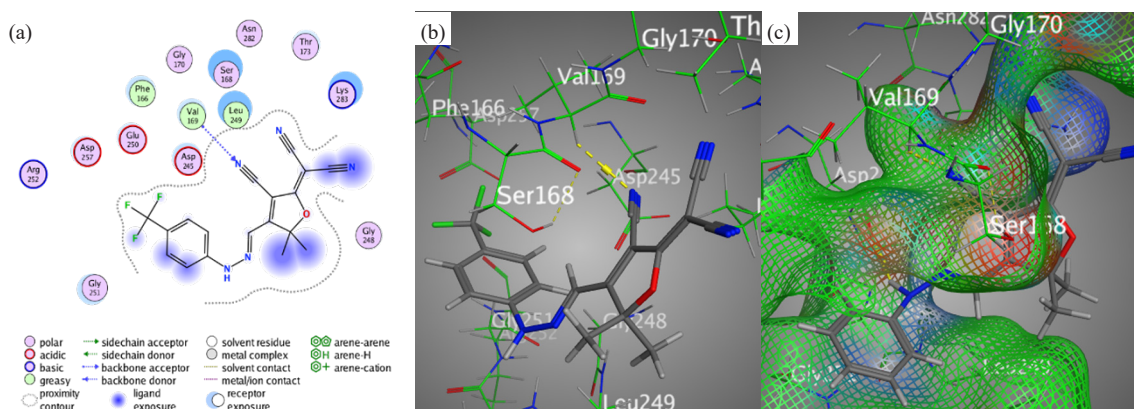


**Figure 6.** Docking interactions between chromophore 4 and PDB: 1lnz. (a) 2D, (b) 3D, (c) Surface Mapping. PDB: Protein data bank.

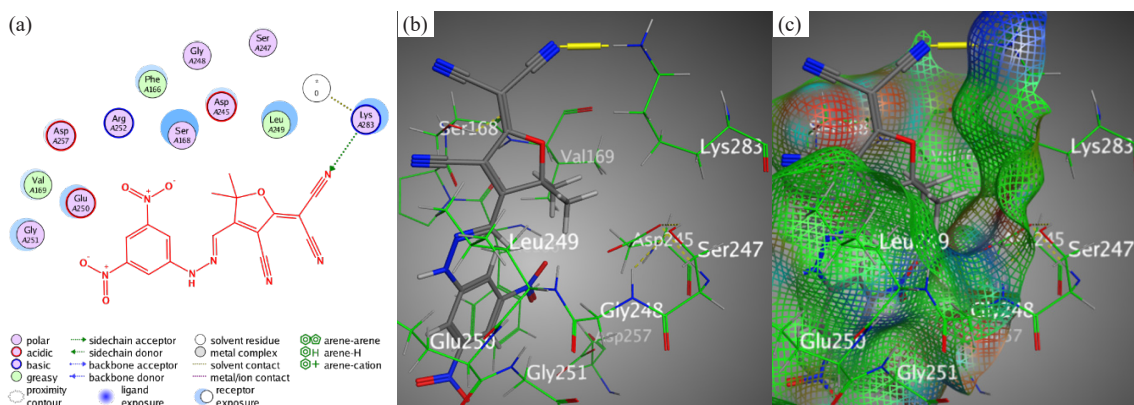


**Figure 7.** Docking interactions between chromophore 5 and PDB: 1lnz. (a) 2D, (b) 3D, (c) Surface Mapping. PDB: Protein data bank.

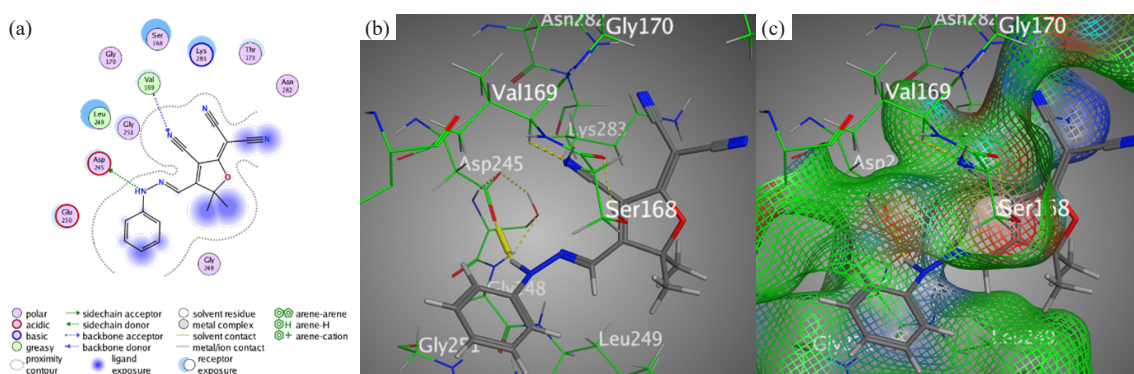


**Figure 8.** Docking interactions between chromophore 1 and PDB: 1lnz. (a) 2D, (b) 3D, (c) Surface Mapping. PDB: Protein data bank.

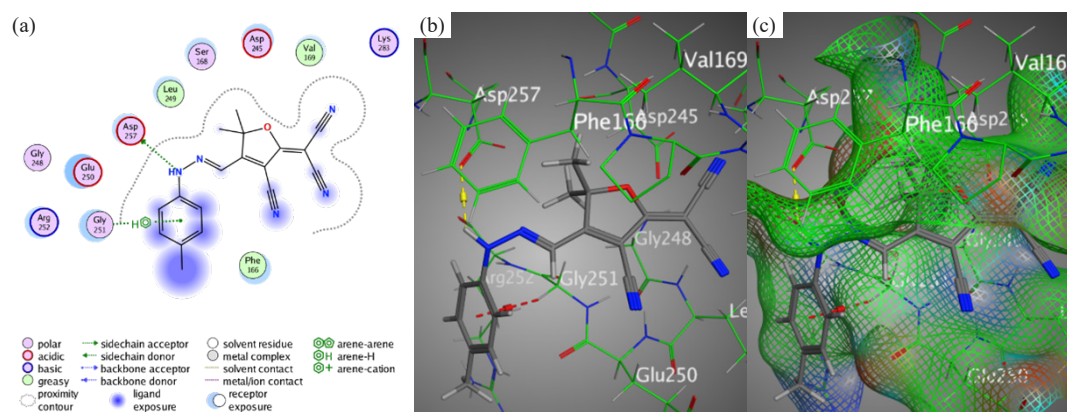


**Figure 9.** Docking interactions between chromophore 2 and PDB: 1lnz. (a) 2D, (b) 3D, (c) Surface Mapping. PDB: Protein data bank.

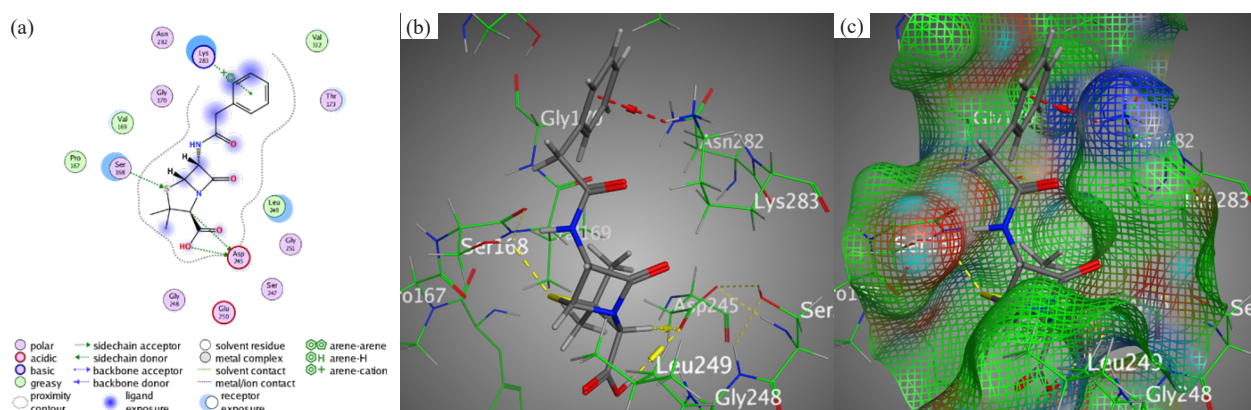


**Figure 10.** Docking interactions between Penicillin and PDB: 1lnz. (a) 2D, (b) 3D, (c) Surface Mapping. PDB: Protein data bank.

The main interaction bindings in chromophore 4 were the formation of H-acceptor bond between Val169 and the nitrile group's N24. These results underscore the diversity of ligand-protein interactions and their role in determining binding affinity overall. Additionally, molecular docking analysis revealed that penicillin had binding energy (S) of -6.0265 kcal/mol and an Rmsd magnitude of 1.4275 due to hydrogen bonding interactions between the thiazolidinone ring and Asp245 (H-donor), the carboxylic acid's O12 and Asp245 (H-donor), the thiazolone ring's S7 and Ser168 (H-acceptor) (Figure 10), and the phenyl ring and Lys283 ( $\pi$ -cation interaction).

### 3.5. Swiss ADME prediction

Regardless, the pharmacokinetic parameters of supposed drug candidates are important analysts of their efficacy and safety profiles. The results showed that the synthesized tricyanofuran-hydrazone chromophores had differences in their molecular weight, topological polar surface area (TPSA), hydrogen bond donor (HBD), lipophilicity, and acceptor (HBA) sums, and rotatable bonds (RT) (Table 3). However, chromophore 1, with a molecular weight of 303.32 and an iLog P value of 1.86, has a moderate molecular size and low lipophilicity, indicating that it may be acceptable solubility. It has a hydrogen bond donor and five H-bond acceptors, showing the ability to make important interactions with biological targets. The topological polar surface area (TPSA) of 104.99 Å<sup>2</sup> confirms the moderate polarity. With three rotatable bonds and no Lipinski violations, this chromophore meets the drug-likeness criterion. A bioavailability score of 0.55 indicates a modest possibility of absorption and availability for pharmacological action. Comparable to chromophore 1, chromophore 2 has a similar molecular weight (317.34) and lipophilicity (iLog P of 2.38), suggesting alike solubility and membrane permeability. It has the same biological interaction potential as before, with a H-bond donor and five H-bond acceptors. The TPSA stays at 104.99 Å<sup>2</sup>, showing the same quantity

**Table 3.** Swiss ADME results of tricyanofuran-hydrazone chromophores.

Chromophore	M.w	iLog P	HBA	HBD	TPSA	RT	LV	BS
(1) R= H	303.32	1.86	5	1	104.99	3	0	0.55
(2) R= 4-CH <sub>3</sub>	317.34	2.38	5	1	104.99	3	0	0.55
(3) R= 4-(CH <sub>2</sub> ) <sub>2</sub> CH <sub>3</sub>	415.53	3.65	5	1	104.99	10	0	0.55
(4) R= 4-CF <sub>3</sub>	371.32	2.21	8	1	104.99	4	0	0.55
(5) R= 3,5-(NO <sub>2</sub> ) <sub>2</sub>	393.31	1.11	9	1	196.63	5	1	0.55

M.w: Molecular weight, TPSA: Topological polar surface area, LV: Lipinski violations, BS: Bioavailability score, HBD: Hydrogen bond donor, HBA: Hydrogen bond acceptor, iLog P: Lipophilicity parameter, RT: Rotatable bond.

of polarity. Parallel to chromophore 1, it has three rotatable bonds and follows Lipinski's rule without exception. The bioavailability score of 0.55 indicates a comparable level of bioavailability. Meanwhile, chromophore 3 displayed a molecular weight (415.53) and lipophilicity (iLog P = 3.65). Despite this, it has the same number of H-bond acceptors (5) and donors (1) as chromophores 1 and 2, indicating a parallel potential for biological interactions. However, with 10 rotatable H-bonds, it has more conformational flexibility, which may affect its pharmacokinetic characteristics. Despite its larger size, chromophore 3 tracks Lipinski's rule and has a bioavailability score of 0.55. Furthermore, chromophore 4 has a molecular weight of 371.32 and an iLog P value of 2.21, making it parallel to chromophores 1 and 2 but with significantly higher lipophilicity. It has a larger number of H-bond acceptors (8), which might improve its capacity to interact with biological targets. However, it only has one H-bond donor. This chromophore follows Lipinski's rule without exception and has four rotatable bonds, suggesting considerable flexibility. The bioavailability score of 0.55 indicates that chromophores 1 and 2 have a comparable chance of bioavailability. Chromophore 5 exhibited a molecular weight (393.31) and TPSA of 196.63 Å<sup>2</sup> among the investigated chromophores.

Notwithstanding its very low lipophilicity (iLog P = 1.11), it has nine H-bond acceptors and an H-bond donor, designating the possibility of significant H-bonding interactions with biological targets. However, higher TPSA and enhanced polarity may influence its dispersion and permeability characteristics. It commits one Lipinski violation due to the increased number of hydrogen bond acceptors. Nonetheless, it has a bioavailability score of 0.55, designating a modest probability of bioavailability.

Finally, each chromophore has separate molecular characteristics that impact its pharmacokinetic and pharmacodynamic performance. While chromophores 1-4 have mediated molecular weights and lipophilicity, chromophore 5 demonstrates different attributes due to its larger molecular weight and polarity. These variances highlight the need to take individual molecular behaviors into account when designing and developing drugs.

#### 4. Conclusions

New tricyanofuran-hydrazone chromophores were synthesized and analyzed by different spectroscopic techniques. The synthesized hydrazones showed solvatochromism in different organic solvents. The tricyanofuran-hydrazone chromophore was immobilized onto a paper strip for sensing toxic ammonia. The strong electron-withdrawing tricyanofuran group promoted a proton transfer from the hydrazone moiety to ammonia, allowing a colorimetric shift from purple to yellow upon exposure to ammonia vapor. This paper sensor showed high sensitivity in detecting ammonia vapor with good reversibility. Meanwhile, the antimicrobial effectiveness of the newly synthesized tricyanofuran-hydrazone chromophores exhibited that chromophore 5 exhibited the most effective antimicrobial activity among all established chromophores, with MIC values < 38 µg/mL for *S. aureus*, < 71 µg/mL for *S. pneumoniae*, < 122 µg/mL for *E. coli*, < 198 µg/mL for *C. albicans*, and < 226 µg/mL for *A. fumigatus*. These conclusions designate that chromophore 5 is a highly attractive applicant for further development as an antibacterial agent. The wide-ranging effectiveness of this chromophore against Gram-negative, Gram-positive bacteria, and fungi, suggests its potential for combating several infectious disorders. Moreover, a molecular docking investigation provided valuable information about the specific binding interactions between different chromophores and the PDB-1lnz protein. Chromophore 3 displayed the most binding affinity at  $S = -7.2496$  kcal/mol, primarily due to hydrogen bonding between the N 28 of its nitrile group and Asn282. This interaction indicates a robust and precise connection within the binding pocket because of its strong attraction and favorable distance of 3.49 Å between the molecules. Furthermore, the creation of H-bonds between Lys283 and N22 of its nitrile group in chromophore 5 demonstrated a strong binding affinity of  $S = -7.0952$  kcal/mol. This backs up the idea that certain H-bonding interactions are necessary to keep the ligand stable in the active region of the PDB: 1lnz protein, which makes it better at binding. In chromophore 4, the H-acceptor interactions between N 24 of nitrile and Val169 became even more important ( $S = -6.5070$  kcal/mol). Even though the bindings in chromophores 3 and 5 are stronger, these interactions are very important for keeping the ligand at the binding site and maintaining the ligand-protein complex stability. Furthermore, the study underscored the diversity of interactions across the synthesized chromophores, such as  $\pi$ -interactions and various H-bonding forces, illustrating the complex nature of ligand binding. These interactions collectively influence the binding affinities and highlight the importance of considering multiple interaction types when evaluating ligand efficacy.

#### CRedit authorship contribution statement

**Salhah D. Al-Qahtani:** Conceptualization, Methodology, Visualization, Investigation, Supervision, Data curation, Software, Validation, Writing-Original draft preparation, Writing-Reviewing and Editing. **Ghadah M. Al-Senani:** Conceptualization, Methodology, Data curation, Writing-Reviewing and Editing. **Maryam Aldoghaim:** Conceptualization, Methodology, Data curation, Writing-Original draft preparation.

#### Declaration of competing interest

The authors declare that they have no competing interests.

#### Declaration of Generative AI and AI-assisted technologies in the writing process

The authors confirm that there was no use of artificial intelligence (AI)-assisted technology for assisting in the writing or editing of the manuscript and no images were manipulated using AI.

#### Acknowledgment

Princess Nourah bint Abdulrahman University Researchers Supporting Project number (PNURSP2025R122), Princess Nourah bint Abdulrahman University, Riyadh, Saudi Arabia.

#### Supplementary data

Supplementary material to this article can be found online at [https://dx.doi.org/10.25259/AJC\\_72\\_2025](https://dx.doi.org/10.25259/AJC_72_2025).

#### References

- Sharma, P.C., Sharma, D., Sharma, A., Saini, N., Goyal, R., Ola, M., Chawla, R., Thakur, V.K., 2020. Hydrazone comprising compounds as promising anti-infective agents: Chemistry and structure-property relationship. *Materials Today Chemistry*, **18**, 100349. <https://doi.org/10.1016/j.mtchem.2020.100349>
- Murugappan, S., Dastari, S., Jungare, K., Barve, N.M., Shankaraiah, N., 2024. Hydrazone-hydrazone as enabling linkers in anti-cancer drug discovery: A comprehensive review. *Journal of Molecular Structure*, **1307**, 138012. <https://doi.org/10.1016/j.molstruc.2024.138012>
- Popiołek, Ł., 2021. The bioactivity of benzenesulfonyl hydrazones: A short review. *Biomedicine & Pharmacotherapy = Biomedecine & Pharmacotherapie*, **141**, 111851. <https://doi.org/10.1016/j.biopha.2021.111851>
- Devi, J., Kumar, B., Taxak, B., 2022. Recent advancements of organotin (IV) complexes derived from hydrazone and thiosemicarbazone ligands as potential anticancer agents. *Inorganic Chemistry Communications*, **139**, 109208. <https://doi.org/10.1016/j.inoche.2022.109208>
- Ayyannan, G., Mohanraj, M., Gopiraman, M., Uthayamalar, R., Raja, G., Bhuvanesh, N., Nandhakumar, R., Jayabalakrishnan, C., 2020. New palladium(II) complexes with ONO chelated hydrazone ligand: Synthesis, characterization, DNA/BSA interaction, antioxidant and cytotoxicity. *Inorganica Chimica Acta*, **512**, 119868. <https://doi.org/10.1016/j.ica.2020.119868>
- Çakmak, R.Şit, Başaran, E.İp, Kaya, S.Ş, Erkan, S., 2022. Synthesis, spectral characterization, chemical reactivity and anticancer behaviors of some novel hydrazone derivatives: Experimental and theoretical insights. *Journal of Molecular Structure*, **1253**, 132224. <https://doi.org/10.1016/j.molstruc.2021.132224>
- Latrache, M., Hoffmann, N., 2021. Photochemical radical cyclization reactions with imines, hydrazones, oximes and related compounds. *Chemical Society Reviews*, **50**, 7418-7435. <https://doi.org/10.1039/d1cs00196e>
- Khattab, T.A., 2020. From chromic switchable hydrazones to smart materials. *Materials Chemistry and Physics*, **254**, 123456. <https://doi.org/10.1016/j.matchemphys.2020.123456>
- Omidi, S., Kakanejadifard, A., 2020. A review on biological activities of Schiff base, hydrazone, and oxime derivatives of curcumin. *RSC Advances*, **10**, 30186-30202. <https://doi.org/10.1039/d0ra05720g>
- Gebretsadik, T., Yang, Q., Wu, J., Tang, J., 2021. Hydrazone based spin crossover complexes: Behind the extra flexibility of the hydrazone moiety to switch the spin state. *Coordination Chemistry Reviews*, **431**, 213666. <https://doi.org/10.1016/j.ccr.2020.213666>
- Khattab, T.A., 2018. Novel solvatochromic and halochromic sulfahydrazone molecular switch. *Journal of Molecular Structure*, **1169**, 96-102. <https://doi.org/10.1016/j.molstruc.2018.05.048>
- Ding, Y., Guo, X., Du, B., Hu, X., Yang, X., He, Y., Zhou, Y., Zang, Z., 2021. Low-operating temperature ammonia sensor based on Cu<sub>2</sub>O nanoparticles decorated with p-type MoS<sub>2</sub> nanosheets. *Journal of Materials Chemistry C*, **9**, 4838-4846. <https://doi.org/10.1039/d1tc00391g>
- Jin, L., Wu, C., Wei, K., He, L., Gao, H., Zhang, H., Zhang, K., Asiri, A.M., Alamry, K.A., Yang, L., Chu, X., 2020. Polymeric Ti<sub>3</sub>C<sub>2</sub>T<sub>x</sub> MXene composites for room temperature ammonia sensing. *ACS Applied Nano Materials*, **3**, 12071-12079. <https://doi.org/10.1021/acsnano.0c02577>
- Insausti, M., Timmis, R., Kinnersley, R., Rufino, M.C., 2020. Advances in sensing ammonia from agricultural sources. *The Science of the Total Environment*, **706**, 135124. <https://doi.org/10.1016/j.scitotenv.2019.135124>
- Wang, D., Zhang, D., Yang, Y., Mi, Q., Zhang, J., Yu, L., 2021. Multifunctional latex/Polytetrafluoroethylene-based triboelectric nanogenerator for self-powered organo-like MXene/Metal-Organic framework-derived CuO nanohybrid ammonia sensor. *ACS Nano*, **15**, 2911-19. <https://doi.org/10.1021/acsnano.0c09015>

16. Tang, X., Raskin, J.-P., Kryvutsa, N., Hermans, S., Slobodian, O., Nazarov, A.N., Debliqy, M., 2020. An ammonia sensor composed of polypyrrole synthesized on reduced graphene oxide by electropolymerization. *Sensors and Actuators B: Chemical*, **305**, 127423. <https://doi.org/10.1016/j.snb.2019.127423>
17. Zhang, S., Wang, J., Torad, N.L., Xia, W., Aslam, M.A., Kaneti, Y.V., Hou, Z., Ding, Z., Da, B., Fatehmulla, A., Aldhafiri, A.M., Farooq, W.A., Tang, J., Bando, Y., Yamauchi, Y., 2020. Rational design of nanoporous moS<sub>2</sub>/V<sub>2</sub>S<sub>3</sub> heteroarchitecture for ultrahigh performance ammonia sensors. *Small (Weinheim an der Bergstrasse, Germany)*, **16**, e1901718. <https://doi.org/10.1002/smll.201901718>
18. Zhai, X., Wang, X., Zhang, J., Yang, Z., Sun, Y., Li, Z., Huang, X., Holmes, M., Gong, Y., Povey, M., Shi, J., Zou, X., 2020. Extruded low density polyethylene-curcumin film: A hydrophobic ammonia sensor for intelligent food packaging. *Food Packaging and Shelf Life*, **26**, 100595. <https://doi.org/10.1016/j.fpsl.2020.100595>
19. Ricci, P.P., Gregory, O.J., 2021. Sensors for the detection of ammonia as a potential biomarker for health screening. *Scientific Reports*, **11**, 7185. <https://doi.org/10.1038/s41598-021-86686-1>
20. Zhang, D., Yu, S., Wang, X., Huang, J., Pan, W., Zhang, J., Meteku, B.E., Zeng, J., 2022. UV illumination-enhanced ultrasensitive ammonia gas sensor based on (001)TiO<sub>2</sub>/MXene heterostructure for food spoilage detection. *Journal of Hazardous Materials*, **423**, 127160. <https://doi.org/10.1016/j.jhazmat.2021.127160>
21. Aarya, S., Kumar, Y., Chahota, R.K., 2020. Recent advances in materials, parameters, performance and technology in ammonia sensors: A review. *Journal of Inorganic and Organometallic Polymers and Materials* **30**, 269-290. <https://doi.org/10.1007/s10904-019-01208-x>
22. Bielecki, Z., Stacewicz, T., Smulko, J., Wojtas, J., 2020. Ammonia gas sensors: Comparison of solid-state and optical methods. *Applied Sciences*, **10**, 5111. <https://doi.org/10.3390/app10155111>
23. Li, D., Xu, X., Li, Z., Wang, T., Wang, C., 2020. Detection methods of ammonia nitrogen in water: A review. *TrAC Trends in Analytical Chemistry*, **127**, 115890. <https://doi.org/10.1016/j.trac.2020.115890>
24. Kumar, V., Mirzaei, A., Bonyani, M., Kim, K.-H., Kim, H.W., Kim, S.S., 2020. Advances in electrospun nanofiber fabrication for polyaniline (PANI)-based chemoresistive sensors for gaseous ammonia. *TrAC Trends in Analytical Chemistry*, **129**, 115938. <https://doi.org/10.1016/j.trac.2020.115938>
25. Kwak, D., Lei, Y., Maric, R., 2019. Ammonia gas sensors: A comprehensive review. *Talanta*, **204**, 713-730. <https://doi.org/10.1016/j.talanta.2019.06.034>
26. Chatterjee, B., Bandyopadhyay, A., 2016. Development of zinc oxide sensors for detecting ammonia gas in the ambient air: A critical short review. *Environmental Quality Management*, **26**, 89-105. <https://doi.org/10.1002/tqem.21483>
27. Elsayy, H., Sedky, A., Abou Taleb, M.F., El-Newehy, M.H., 2022. Preparation of novel reversible thermochromic polyethylenimine dendrimer and tricyanofuran hydrazone chromophore. *European Polymer Journal*, **174**, 111344. <https://doi.org/10.1016/j.eurpolymj.2022.111344>
28. Gaffer, H.E., Althagafi, I.I., 2020. Synthesis of new azobenzene dyes clubbed with thiazolidinone moiety and their applications. *Pigment & Resin Technology*, **49**, 207-214. <https://doi.org/10.1108/prt-02-2019-0022>
29. Kaushal, M., Lobana, T.S., Nim, L., Kaur, J., Bala, R., Hundal, G., Arora, D.S., Garcia-Santos, I., Duff, C.E., Jasinski, J.P., 2018. Synthesis, structures, antimicrobial activity and biosafety evaluation of pyridine-2-formaldehyde-*N*-substituted-thiosemicarbazones of copper(ii). *New Journal of Chemistry*, **42**, 15879-15894. <https://doi.org/10.1039/c8nj03619e>
30. Alsaedi, H., 2023. Synthesis, characterization, antibacterial activity, and molecular docking of novel dicyanodihydrofuran-based push-pull fluorophores. *Luminescence*, **38**, 527-535. <https://doi.org/10.1002/bio.4477>
31. El-Newehy, M.H., El-Hamshary, H., Salem, W.M., 2021. Solution blowing spinning technology towards green development of urea sensor nanofibers immobilized with hydrazone probe. *Polymers*, **13**, 531. <https://doi.org/10.3390/polym13040531>
32. Khattab, T.A., Tiu, B.D.B., Adas, S., Bunge, S.D., Advincula, R.C., 2016. Solvatochromic, thermochromic and pH-sensory DCDHF-hydrazone molecular switch: Response to alkaline analytes. *RSC Advances*, **6**, 102296-102305. <https://doi.org/10.1039/c6ra24113a>
33. Reichardt, C., 1994. Solvatochromic dyes as solvent polarity indicators. *Chemical Reviews*, **94**, 2319-2358. <https://doi.org/10.1021/cr00032a005>